IOP PUBLISHING PHYSICS IN MEDICINE AND BIOLOGY

Phys. Med. Biol. **55** (2010) 1719–1734 doi:10.1088/0031-9155/55/6/012

Computer-assisted analysis of peripheral zone prostate lesions using T2-weighted and dynamic contrast enhanced T1-weighted MRI

Pieter C Vos, Thomas Hambrock, Jelle O Barenstz and Henkjan J Huisman

Department of Radiology, Radboud University Medical Centre, Nijmegen, 6525GA, The Netherlands

E-mail: p.vos@rad.umcn.nl

Received 15 December 2008, in final form 5 February 2010
Published 2 March 2010
Online at stacks.iop.org/PMB/55/1719

Abstract

In this study, computer-assisted analysis of prostate lesions was researched by combining information from two different magnetic resonance (MR) modalities: T2-weighted (T2-w) and dynamic contrast-enhanced (DCE) T1-w images. Two issues arise when incorporating T2-w images in a computer-aided diagnosis (CADx) system: T2-w values are position as well as sequence dependent and images can be misaligned due to patient movement during the acquisition. A method was developed that computes T2 estimates from a T2-w and proton density value and a known sequence model. A mutual information registration strategy was implemented to correct for patient movement. Global motion is modelled by an affine transformation, while local motion is described by a volume preserving non-rigid deformation based on *B*-splines. The additional value to the discriminating performance of a DCE T1-w-based CADx system was evaluated using bootstrapped ROC analysis. T2 estimates were successfully computed in 29 patients. T2 values were extracted and added to the CADx system from 39 malignant, 19 benign and 29 normal annotated regions. T2 values alone achieved a diagnostic accuracy of 0.85 (0.77–0.92) and showed a significantly improved discriminating performance of 0.89 (0.81–0.95), when combined with DCE T1-w features. In conclusion, the study demonstrated a simple T2 estimation method that has a diagnostic performance such that it complements a DCE T1-w-based CADx system in discriminating malignant lesions from normal and benign regions. Additionally, the T2 estimate is beneficial to visual inspection due to the removed coil profile and fixed window and level settings.

(Some figures in this article are in colour only in the electronic version)

1. Introduction

Several studies have indicated that multimodal MRI increases the prostate cancer (PCa) localization accuracy of the radiologist. The accuracy is, however, dependent on the experience of the radiologist (Hricak *et al* 2007, Futterer *et al* 2006, Chan *et al* 2003). To help improve the diagnostic accuracy of the unexperienced radiologist, we investigated the value of a computer-aided diagnosis (CADx) system. In a previous study (Vos *et al* 2008a), the feasibility of a CADx system was shown that calculates the malignancy likelihood of a given suspicious area in the peripheral zone of the prostate using T1-w DCE-MRI. Discrimination of malignant and benign regions was performed using a support vector machine (SVM) as a classifier that was trained with features extracted from quantitative pharmacokinetic (PK) maps as well as T1 estimates. The study showed that a diagnostic accuracy of 0.83 (0.75–0.92) was obtained by a standalone CADx. It is expected that by adding more MR modalities, the discriminating performance of the CADx system will further improve.

In this paper, the possibility of using T2-w images as an additional MR modality to discriminate PCa from benign regions in the peripheral zone (PZ) of the prostate is studied, as they are also used by the radiologist for localizing PCa. Two issues arise when including the T2-w images in a DCE-based CADx system. First, there can be misalignment of T2-w and DCE images as patient movement between the series is inevitable during a prostate study. Secondly, the acquired T2-w signal intensities are not linearly related to the underlying tissue T2 relaxation times and depend on the 3D spatial position relative to the receiving coil elements. To resolve the nonlinearity, a T2 estimator was used that was published previously (Engelbrecht *et al* 2003, Mulkern *et al* 2004). The approach requires both T2-w, proton density (PD) images and a known sequence model. Note that although the acquisition of quantitative T2 maps is possible using a multi-echo spin echo technique in a reasonable time span on contemporary MR systems, spatial resolution will be considerably lower. Patient movement can be retrospectively corrected by aligning images using image registration, which is necessary for both the T2 estimation and inclusion in the CADx system. In this study a method is proposed that models global shifts with affine transformation and local deformation using B-splines. This method also estimates the coefficients to maximize the mutual information (MI) between the two images. The method is based on the work of Rueckert *et al* (1999) which was further developed and tested by Mattes *et al* (2003). MI-based registration is a common choice to register different modalities and is considered suitable for registration of images that do not have the same pixel intensity range (Studholme *et al* 1997, Maes *et al* 1997, Wells *et al* 1996, Pluim *et al* 2003).

To our knowledge, no studies have been reported about similar work on PCa using DCE-MRI and T2-w images. Chan *et al* (2003) describe the only *in vivo* CADx system that provides an estimated malignancy likelihood using multimodal MRI. They constructed a summary statistical map of the peripheral zone based on the utility of multi-channel statistical classifiers combining textural and anatomical features in PCa areas from T2-w images, diffusion-weighted images (DWI), PD maps and T2 maps. The achieved diagnostic performance of 0.84 is, however, of limited clinical value because the discrimination did not include benign regions such as prostatitis or hemorrhage. Madabhushi *et al* (2005) generated similar statistical maps based on T2-w images using whole mount sections as the 'ground truth' and showed the additional value of combining numerous features. Unfortunately no discrimination performance was calculated, computation time for analysis of one complete MRI scene exceeds an hour and the method is limited to 2D *ex vivo* MRI. Viswanath *et al* (2008) extended the method of Madabhushi *et al* with a non-rigid registration scheme to map PCa whole mount histological sections onto corresponding 2D DCE-MRI. Though the method

potentially improves the objective annotation of PCa, the corresponding slice still needs to be selected. The unsupervised classification by *k*-means clustering achieved an accuracy of 77%. Their advocated methodology is, however, evaluated on a per-pixel basis, whereas the proposed method captures the heterogeneous nature of PCa by using percentiles within a given region (Collins and Padhani 2004, Padhani 2003).

The purpose of this study was to investigate the feasibility of including T2-w MR in a multi-modal computer-aided diagnostic system for prostate MR.

2. Materials and methods

2.1. Patient characteristics

The study set consisted of 34 consecutive patients (mean age, 60 years; range 50–69 years) that were selected in a previous study of Futterer *et al* (2006). These patients had biopsy-proven PCa and underwent DCE-MR imaging at 1.5-T, complementary to the routine staging MR imaging examination of the prostate. Patients were included (between 1 April 2002 and 1 June 2004) in the study only if they were candidates for radical retropubic prostatectomy within 6 weeks after MR imaging. The study of Fütterer *et al* was approved by the institutional review board and informed consent was obtained from all patients prior to MR imaging. After imaging, all patients underwent radical retropubic prostatectomy. Exclusion criteria were previous hormonal therapy, contra-indications to MR imaging (e.g. cardiac pacemakers, intracranial clips), contraindications to endorectal coil insertion (e.g. anorectal surgery, inflammatory bowel disease). The mean prostate-specific antigen level was 8 ng mL^{-1} (range 3.2–23.6 ng mL^{-1}) and the mean Gleason score was 6.1 (range 5–8). MRI was performed on average 3 weeks after transrectal ultrasonographically guided sextant biopsy of the prostate.

2.2. MR protocol

Images were acquired with a 1.5 T whole body MR scanner (Sonata, Siemens Medical Solutions, Erlangen, Germany). A pelvic phased-array coil and a balloon-mounted disposable endorectal surface coil (MedRad®, Pittsburgh, PA, USA, inserted and inflated with approximately 80 cm^3 of air) were used as a receiver. The integrated body coil was used for transmitting. All patients who received 1 mg of glucagon (Glucagon®, Novo Nordisk, Bagsvaerd, Denmark) were administered intramuscularly directly prior to the MRI scan, to reduce peristaltic bowel movement during the examination.

Table 1 shows the sequence parameters. The protocol for acquisition consisted first of a localizer and two fast gradient spin echo measurements for patient and coil positioning verification. Thereafter, high-spatial-resolution T2-w turbo spin echo imaging in the axial, sagittal and coronal planes, covering the prostate and seminal vesicles, was performed. Next, 3D T1-w spoiled gradient echo images were acquired before and during an intravenous bolus injection of paramagnetic gadolinium chelate (0.1 mmol kg^{-1}, gadopentetate, Magnevist®; Schering, Berlin, Germany) using a power injector (Spectris, Medrad®, Pittsburgh, PA, USA) with an injection rate of 2.5 ml s^{-1} followed by a 15 ml saline flush. The recorded repetition time (TR) of 34 ms represents the time to acquire 12 *k*-lines (two of 12 slices were used for oversampling). A 6/8 partial Fourier reconstruction (FFT) was used to reduce the acquisition time. With these settings, complete 3D volumes were acquired every 2 s for a duration of 120 s. Before contrast injection, the same axial 3D T1-w gradient echo sequence, though with a longer TR time without partial Fourier reconstruction, was used to obtain PD-w images at identical positioning to allow calculation of the T2 estimates and the PK parameters. The

Table 1. Parameters for MR imaging.

Sequence	Sequence type	Duration (min)	TR (ms)	TE (ms)	Echo train length	No of averages (NEX)	Flip angle (degree)	Slice thickness (mm)	Matrix	No of slices	Field of view (mm × mm)	Phase-encoding direction	Spatial resolution
T2-w Axial	tse[a]	3m50s	4400	132	15	2	180[b]	4	240 × 512	11–15	132 × 280	R-L[c]	.55 × .55 × 4
T2-w Sagittal	tse	4m 40s	4000	132	15	2	180[b]	4	179 × 512	11–15	100 × 280	A-P[d]	.55 × .55 × 4
T2-w Coronal	tse	4m	4000	132	15	2	180[b]	4	179 × 512	11–15	100 × 280	R-L	.55 × .55 × 4
Dynamic T1-w PD 3D gradient-echo	tfl[e]	1m0s	800	1.6	1	1	8	4	77 × 256	10[f]	240 × 280	A-P	3.1 × 1.1 × 4
Dynamic T1-w fast 3D gradient-echo	tfl	0m2s	34[g]	1.6	1	1	14	4	77 × 256	10[f]	240 × 280	A-P	3.1 × 1.1 × 4

[a] Turbo spin echo.
[b] Refocussing flip angle.
[c] Right-left.
[d] Anterior-posterior.
[e] Turbo flash.
[f] Two of 12 slices used for oversampling.
[g] Represents the time to acquire 12 *k*-lines.

gadolinium concentration curves and PK parameters were calculated as reported by Huisman *et al* (2001). The PK parameter set that was used in this experiment consisted of the pre-contrast static value of the T1 estimate of the longitudinal relaxation rate in (ms) ($T1$ *Static*), the relative size of the extracellular, extravascular space (V_e), the rate constant (k_{ep}) and the transfer constant (K^{trans}). They are described in detail in Vos *et al* (2008a).

2.3. Image registration algorithm

This section describes an image registration method that automatically seeks for an estimate of the transformation $\hat{T}$ that aligns the PD image F and T2-w image M by optimizing a similarity measure S over the transformation T:

$$S(F, M(T)). \tag{1}$$

The registration procedure consisted of several components, the most important of which were the choice of similarity measure, the transformation degrees of freedom and the cost function for similarity of measurement.

2.3.1. Deformation model. An initial alignment of F and M was achieved using a 12 element affine transformation matrix T_{global}, as reported previously (Vos *et al* 2008b). In general, an affine transformation is composed of linear transformations (rotation, scaling or shear) and a translation. It ensures a global registration with low computational costs. An additional transformation T_{local} modelled local deformation. In this work, deformations are modelled on cubic B-splines, because of their computational efficiency (separability in multiple dimensions, calculation via filtering), smoothness, and local control (Rueckert *et al* 1999). A B-spline transformation deforms a volume by manipulating an underlying mesh of control points (D). Deformation is calculated using the positions of a $4 \times 4 \times 4$ neighbourhood of control points and third-order spline polynomials, where the parameters of the B-spline transformation are the coordinates of the control points. In the presented method, the initial T_{global} was used as an offset of T_{local}:

$$T = T_{\text{local}} \cdot T_{\text{global}}. \tag{2}$$

2.3.2. Similarity measure. In this study MI was used as a similarity measure because F and M do not have the same appearance. When F and M are optimally aligned, their MI is maximal:

$$\hat{T} = \arg\min_{\psi}(-MI(\psi)), \tag{3}$$

where $MI(\psi)$ denotes the MI similarity measure as a function of the transformation parameters, ψ. Although several implementations for the computation of MI exists, the presented method is based on the work of Mattes *et al* (2003). Their registration method makes efficient use of the B-spline basis functions that models the deformation field and converges quickly when compared to other methods, due to stochastic sampling (Klein *et al* 2007).

MI relates the joint entropy to the entropies of the modalities separately:

$$MI(\psi) = H(f(x)) + H(m(\psi(x))) - H(f(x), m(\psi(x))), \tag{4}$$

where $H(f(x))$ and $H(m(\psi(x)))$ are the marginal entropies, $H(f, m; \psi)$ is the joint entropy, $f(x)$ and $m(x)$ denote observations of F and M, respectively, and x denotes the voxel coordinate. The joint entropy $H(f, m; \psi)$ uses a set of fixed bin centres in f and moving bin centres in m as initialization.

The entropy of an image is computed from the probability density function (pdf) of the image intensities. Parzen windowing was used to obtain a differentiable pdf. This reduces the effects of quantization from interpolation and discretization from binning the data, see Thévenaz and Unser (2000) for a detailed description. The joint entropy is computed using

$$H(f, m; \psi) = \sum_{x \in X_F} w_f(I_F(x_F) - f) w_m(I_M(g(x_F; \psi)) - m), \tag{5}$$

where $I_F(x_F)$ and $I_M(g(x_F; \psi))$ are samples of the fixed and interpolated moving images, respectively, and w_f and w_m are the Parzen window kernels (Mattes *et al* 2003). To reduce the computational costs, the set of intensity samples (X_F) was set to a randomly selected 20% of the total number of voxels and the joint histogram was calculated based on 100 bins for each image. These settings gave robust results on all experiment data. To further speed up the calculation of the $MI(\psi)$, samples were only drawn from a subregion of F. This will be further discussed in section 2.3.5.

2.3.3. Constraint on the transformation. In addition to the MI similarity measure, a regularization term P was incorporated in the registration method to constrain the deformation of the coordinate space:

$$C(F, M(T)) = -S(F, M(T)) + \alpha P(T), \tag{6}$$

where α is a user-defined weight factor for P, allowing more control over the influence of the regularization term on the overall cost C. Similar to the work of Rohlfing *et al* (2003), a volume preserving constraint was incorporated and implemented by penalizing deviations of the Jacobian determinant J of the deformation from unity, that is, it assumes local rigidity and penalizes local tissue expansion and compression:

$$P(\psi) = \frac{1}{N_D} \sum_{x \in D} |\log(J_\psi(x)|, \tag{7}$$

where D represents the set of control points used for the deformation.

Calculation of the gradient of the constraint is necessary for an efficient and robust optimization (see section 2.3.4). The derivatives were calculated using the common finite-difference approximation:

$$\frac{\delta P}{\delta_i} \approx \frac{P(\psi_i + \delta_i) - P(\psi_i)}{\delta_i}, \tag{8}$$

where δ_i equals 1 mm and the subscript i refers to the parameter index.

2.3.4. Optimization of the cost function. The L-BFGS-B (Zhu *et al* 1997), a limited-memory, quasi-Newton minimization package, was used to optimize the cost function C until termination criteria were satisfied. The limited-memory method is well suited for optimizing the large number of parameters ψ in the B-spline transformation when a high resolution of control points is used. L-BFGS-B provides an additional advantage in that it allows bound constraints (B) on the independent variables. In this manner, maximum displacements of the control points can be controlled. Note that displacements in the slice direction were considered unlikely and therefore restricted with a fixed bound set to 0. The optimization terminates when the change in C between consecutive iterations falls below the tolerance of $1e^{-4}$.

2.3.5. Centered cropped optimization strategy. A high resolution of control points in the *B*-spline transform T comes with high computational costs, due to the high number of displacements of the control points D that needs to be explored. For the intended application, the focus is on the non-rigid displacement of the prostate. Hence, it suffices to limit the registration method to the centre area of the pelvis, where the prostate is situated. The set of control points (D) is defined over the entire volume (F) plus a finite support region of three at the borders, thereby extending the region of interest. Simply defining a smaller mesh inside the volume results in interpolation artefacts near the edges of the grid. Therefore, optimization was limited to a centred subset ($D_R \subset D$) of control points. Because the number of parameters in D_R is much smaller, the registration method becomes considerably faster. The resolution of the grid control points was set to $14 \times 14 \times 8$ (including the finite support region). A centred subregion (D_R) of size $4 \times 4 \times 3$ was chosen such that the prostate area was covered in all cases.

2.4. Histological verification

All patients underwent radical retropubic prostatectomy. From the prostatectomy specimens, whole-mount step-section histology tumour maps were created by an experienced pathologist who was blinded to the imaging results. The whole-mount step-section histology tumour maps were used as ground truth for training and evaluating the performance of the CADx system. The morphologies of the central gland, peripheral zone, cysts, calcifications and urethra were used as landmarks to find the corresponding MRI slice. The anatomy of the prostate is best imaged on T2-w images and is therefore used for correlating the histopathological map. A method was implemented to prevent bias when annotating the ground truth, as described elsewhere (Vos *et al* 2008a). Using this method, regions of normal PZ, PCa, benign PZ tissue (identified as tumour suspicious on T2-w and DCE-MRI but not representing tumour on pathology) and levator ani muscle were outlined manually. The regions that contained muscle were used for the reference tissue method, as explained in section 2.5.

2.5. Quantitative T2 estimation from T2-w and PD series

T2 relaxation times can be computed with a fast method that uses a known sequence signal model as prior knowledge and only a few echo times (TE) to fit the T2 relaxation curve. Hittmair *et al* (1994) presented a method that estimates the T1 relaxation rate with only two repetition times (TR) and a spin echo sequence as a signal model. In this study a comparable approach is applied to estimate the T2 using a T2-w turbo spin echo sequence and PD-w gradient echo sequence. It is assumed that a T2-w sequence is used, such that the TR is much larger than the T1 tissue relaxation times. Then the effect of T1 can be neglected and the received signal s at location x for a T2-w turbo spin echo sequence is

$$s_{t2w}(x) = G_{t2w} \sin(\theta_{t2w}) \rho(x) \exp(-\mathrm{TE}/T2(x)), \tag{9}$$

where G_{t2w} represents the gain setting and θ_{t2w} the excitation flip angle for the T2-w sequence and ρ is a function comprising proton density fluctuations and coil profile at location x. The spatial dependence through $\rho(x)$ models the commonly observed spatial inhomogeneity that is caused by the receive and send coil sensitivity profiles. In the case of a PD-w image, the effect of T1 and T2 should be reduced when TE is set short and TR is set long. Assuming that both sequences use the same coil setup ($\rho(x)$ is identical), the received PD signal can be approximated by

$$s_{pd}(x) = G_{pd} \sin(\theta_{pd}) \rho(x), \tag{10}$$

where G_{pd} is the gain setting and θ_{pd} is the excitation flip angle for the PD-w gradient echo sequence. The $T2$ at position x is derived by rewriting equations (9) and (10):

$$T2(x) = \frac{-\mathrm{TE}}{\log(s_{t2w}(x)) - \log(s_{pd}(x)) - \log(\eta_{t2w,pd})}, \tag{11}$$

where $\eta_{t2w,pd}$ is the gain ratio of $G_{t2w}\sin(\theta_{t2w})$ to $G_{pd}\sin(\theta_{pd})$. In theory, η can be estimated from the MR sequences parameters, but the data were not stored in the DICOM header provided by the MR system. Furthermore, any coil profile artefacts, differences in voxel size, TR or receiver bandwidth can still result in acquisition-to-acquisition signal intensity variations, in spite of the fact that commercial MR systems are nowadays equipped with internal calibration methods. These variations are captured in η and need to be estimated from the data. Therefore, an estimator for the gain ratio $\eta_{t2w,pd}$ was built using a reference tissue R_{ref} with the known T2 value from the literature. In this study the levator ani muscle was used (35.3 ± 3.85 ms at 1.5 T and 37 °C (Gold *et al* 2004)). The gain setting can now be found by performing least-squares optimization using the data from all pixels within the annotated reference tissue:

$$\eta_{\mathrm{opt}} = \arg\min_{\eta} \sum_{x \in R_{\mathrm{ref}}} (T2(x;\eta) - 35)^2. \tag{12}$$

The least-squares procedure that was used, uses Brent's method of parabolic interpolation, protected by golden-section subdivisions if the interpolation is not converging.

2.6. Training and validation

The CADx system extracts a PK and T2 feature set from a region of interest (ROI) using percentiles. The extracted set of features is presented to a trained SVM which calculates the malignancy likelihood for a lesion. The calculated likelihood is presented to a radiologist to assist in his or her diagnosis. The CADx system was implemented in an open source programming environment: the Visualization ToolKit (VTK) using the Tool Command Language (Tcl) and C++.

The discriminating performance of the CADx system was estimated using the area under the receiver operator characteristics (ROC) curve (AUC). Classification was performed using SVM analysis on the feature set (provided by the statistical package R (Hornik 2005))

A prospective-performance estimate of the lesion analysis was made by means of leave-one-patient-out (LOPO) cross-validation. LOPO avoids training and testing on the same data, estimating the likelihoods of ROIs in that left-out case and repeating the procedure until each case has been tested individually. This study was a diagnostic assessment with patient-clustered data; therefore, a bootstrap resampling approach with 10 000 iterations was used for estimating the mean AUCs and 95% confidence intervals, as proposed by Rutter (2000).

The intent of this study was not to provide a new T2 estimator. Nevertheless, some validation was performed to research the validity of the T2 estimates. First, visual inspection was performed. Secondly, the median and variation for T2 relaxation time of the normal peripheral zone were computed. The results were compared with those found in the literature. Thirdly, the method was compared with a multi-echo spin echo sequence, where the T2 relaxation curve was automatically fitted by a Siemens mono-exponential decay fitting algorithm. The sequence settings were seven echo times (15.6–109.2 ms), a spatial resolution of 1.2 × 1.2 × 3.0 mm, matrix of 192 × 96, field of view of 230 × 115, TR of 2080, flipangle of 180 and 16 slices. The levator ani muscle was used as reference and the mean relaxation time was calculated for muscle, benign PZ, fat, normal PZ, normal transition zone (TZ) and lesion PZ in a random patient case. Linear regression and Pearson correlation statistics were performed.

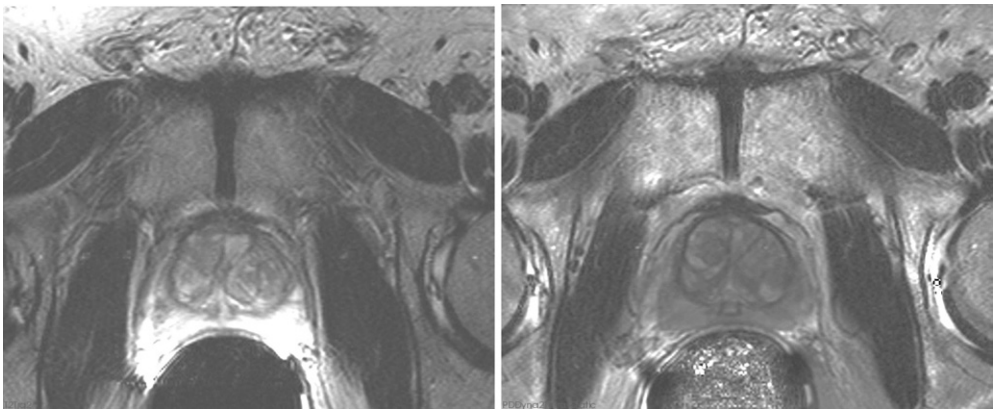

Figure 1. The left T2-w image of the prostate demonstrates the coil sensitivity of conventional MR images. Voxels near the endorectal coil are more intense compared to voxels that are ventrally located. The right image shows the computed T2 image. Note that the coil profile is strongly reduced.

The effect of registration on the diagnostic performance of the CADx system was studied. In this experiment, T2-w values, T2 estimates without registration, T2 estimates after affine registration and T2 estimates after the implemented non-rigid registration were extracted from the annotated regions and tested for their discriminative value. In the following experiment, the effect of parameter settings on the diagnostic performance was valuated. The method was tested with different constraint settings (B) and various Jacobian weighting factors (α), to search for the optimal discriminative performance. In the final experiment the additional discriminative value of T2 estimates in a multimodal setup was tested and compared with the performance of the previous developed CADx system.

3. Results

In total, 34 consecutive patients with histologically proven adenocarcinoma of the prostate were recruited. Four patient studies were excluded because of bad dynamic data caused by large patient movement, coil artefacts and one due to large noise values. In total 39 malignant regions were annotated in the peripheral zone. The number of benign regions annotated in the peripheral zone was 19. The number of annotated regions in the normal peripheral zone was 29.

Figure 1 shows an example case, where the coil profile is prominently visible in the T2-w image but is removed by the method in the quantitative T2 image.

In figure 2 the value of non-rigid registration is demonstrated. Patient movement during the examination and internal (bowel) movement were corrected by the method.

The median calculated T2 relaxation time was 82 ± 7.5 ms for normal PZ, 68 ± 15.4 ms for benign regions and 60 ± 6.9 ms for malignant regions, at the best possible setting of the registration method and using the levator ani muscle as reference tissue. In figure 3, the T2 values of several tissues of one patient case are shown and compared to a Siemens T2 sequence acquired in that same study. A significant linear correlation can be observed.

Figure 4 shows the histograms of the distributions of the T2-w values, T2 estimates without registration, T2 estimates after affine registration and T2 estimates after non-rigid

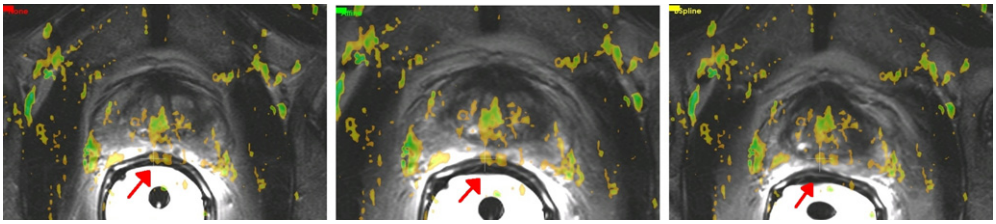

Figure 2. Sample images illustrating the necessity for nonrigid registration. The acquired T2-w image (background image) and the PK parameter K^{trans} (colour-coded transparent overlay) are misaligned in the first image. Typical enhancement patterns are observed periurethral (arrow) and at the neurovascular bundles, but due to patient movement during the examination, the enhancement patterns do not match the underlying T2-w image (left). This can also be observed in the figure in the middle which shows the result of an affine registration, where after a global correction the neurovascular bundles match the enhancement patterns, but a periurethral mismatch is still present. The right image shows the result of the non-rigid registration method. Note the correct location of enhancement at the periurethral region.

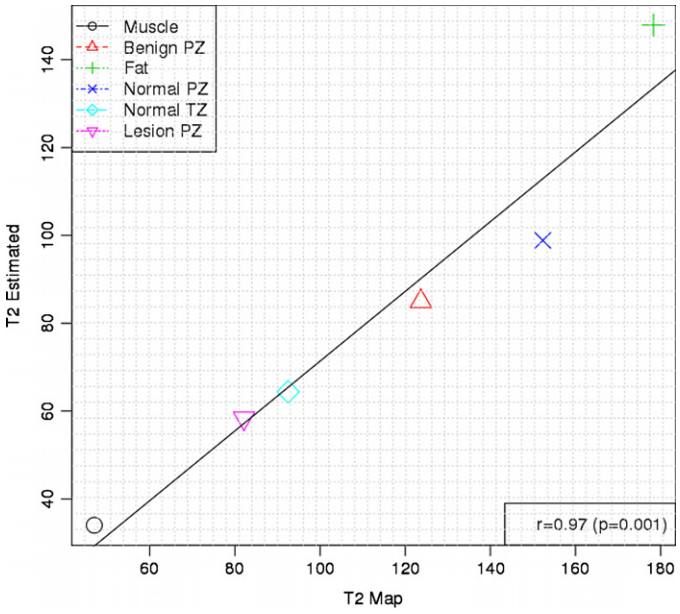

Figure 3. Plot showing the mean T2 relaxation times for several tissues in a patient case, with T2 values generated by a traditional multi-echo sequence of the MR system on the x-axis and on the y-axis and the T2 values generated by the proposed method. The linear regression model and the Pearson correlation statistics are shown.

registration that were extracted from all normal, benign and malignant regions. It can be observed that the amount of overlap between the distributions (especially M and N) is lowest after the non-rigid registration.

Figure 6 shows the effect of varying the parameters α and B on the registration method. At low Jacobian weighting factors ($\alpha < 1.5$), the algorithm tends to be sensitive to the settings of B. Best settings were found at $B = \pm 25$ mm and $\alpha = 1.5$. With these parameter settings, the diagnostic value of the T2 estimates was quantified by the discriminating performance of the

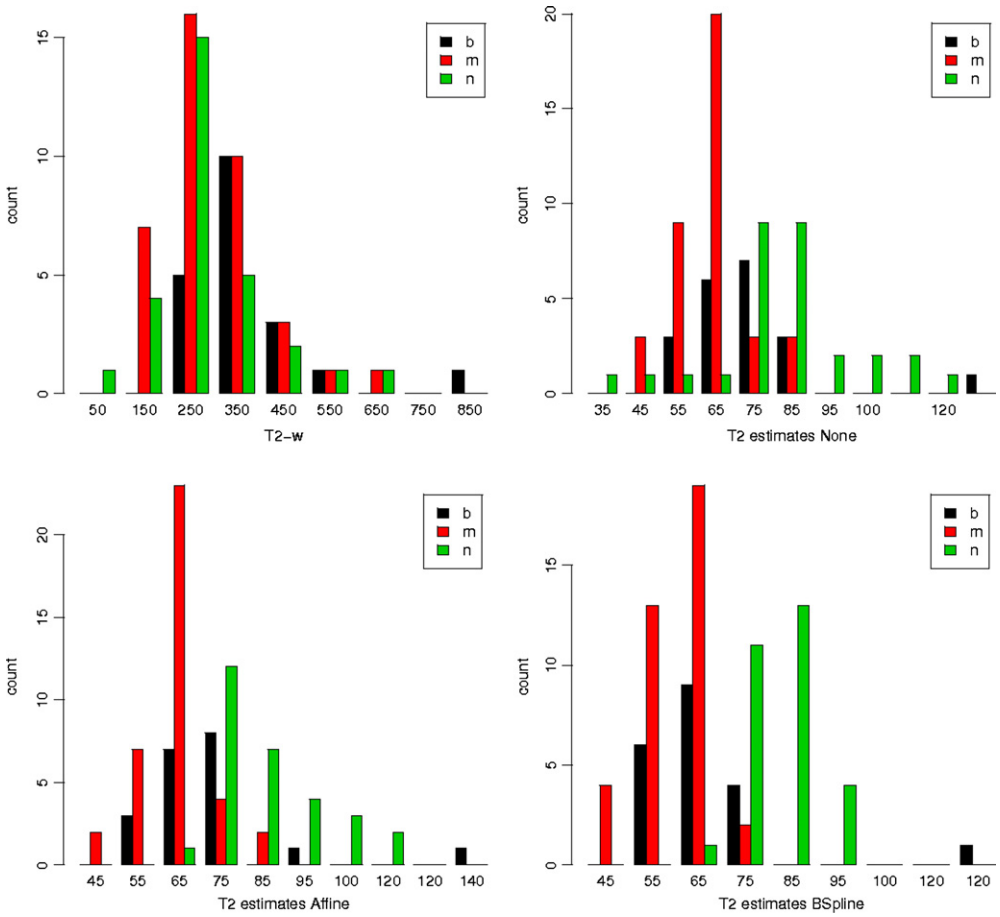

Figure 4. Histograms of T2-w values, T2 estimates without registration (None), T2 estimates using affine registration and T2 estimates using *B*-spline registration. Here, green represents all normal PZ regions, black represents all benign regions and red all malignant regions of the database.

CADx system. In a tumour localization setup, where normal PZ regions were discriminated from benign and malignant regions, a diagnostic performance of 0.97 (0.94–1.00) was achieved using non-rigid registration, as shown in figure 5. Using the non-rigid registration method, a significant improvement was shown compared to the affine registration method, as well as to not using registration. The T2-w values were of no diagnostic value to the CADx system. In a differentiation setup, where normal and benign PZ regions were discriminated from malignant PZ regions, the CADx system achieved a diagnostic performance of 0.85 (0.77–0.92) after non-rigid registration (figure 5). This accuracy was significantly better than not using registration ($p = 0.03$), but did not show a significant improvement to an affine registration.

The accuracy of the CADx system for discriminating normal PZ and benign regions from malignant regions was 0.84 (0.76–0.92) using the PK parameters alone. Adding the estimated T2 relaxation times to the PK feature set resulted in an accuracy of 0.89 (0.81–0.95), which was a significant improvement ($p = 0.03$) (figure 7).

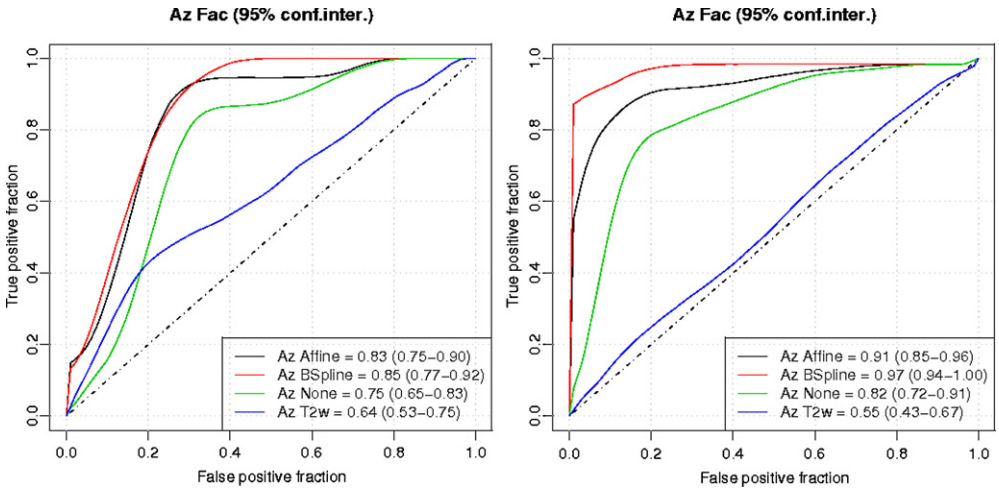

Figure 5. ROC curves showing the discriminating performance of the CADx system using T2 estimates and T2-w values. The T2 estimates were first extracted when no registration was applied, second after affine registration and third after non-rigid registration. The left graph shows the result at a differentiation setup, where PZ and benign PZ regions are discriminated from malignant PZ regions. It can be noted that normal PZ and benign regions are well differentiable from malignant regions. The right graph demonstrates the discriminating performance in a localization setup, where normal PZ is differentiated from both benign regions and malignant regions.

4. Discussion

This study showed the feasibility of including T2-w MR in a multi-modal CADx system for prostate MR. T2 estimates were shown to be of a significant additional diagnostic value for the in-house developed CADx system (Vos *et al* 2008a). Moreover, coil profile sensitivity, that was present in the T2-w images, was noticeably diminished, making these images potentially more beneficial for clinical interpretation during diagnostic viewing.

Registration had a strong influence on the diagnostic performance of the T2 estimates in discriminating normal and benign from malignant regions. This study is unique in comparing registration methods on the actual effect upon the diagnostic performance. While the most registration literature is limited to visual observation or simulated deformations, the present study quantified the effect upon the diagnostic performance. The effect is demonstrated in figure 5. The non-rigid registration method showed the highest diagnostic accuracy. As an example, figure 2 illustrates organ movement that could not be compensated for using affine registration, but was resolved by free form deformation using cubic *B*-splines (Rueckert *et al* 1999). A disadvantage of this technique is that it can lead to loss of topology. Therefore, the Jacobian determinant as a volume preserving constraint on the transformation was included. Figure 6 demonstrates that including such a constraint, the diagnostic performance of the CADx system improves and leads to a more robust registration, as it is less dependent on other parameter settings.

The T2 estimator in this study is a novel, simple method in a CADx context. Although a full validation is outside the scope of this study, some aspects indicate validity. First, visual inspection showed that the coil profile was removed. Secondly, the inter-patient variability of T2 estimates in the normal PZ was small ($\pm$7.5 ms). Thirdly, a significant linear correlation was shown between the T2 estimates of our method and the multi-echo spin echo sequence

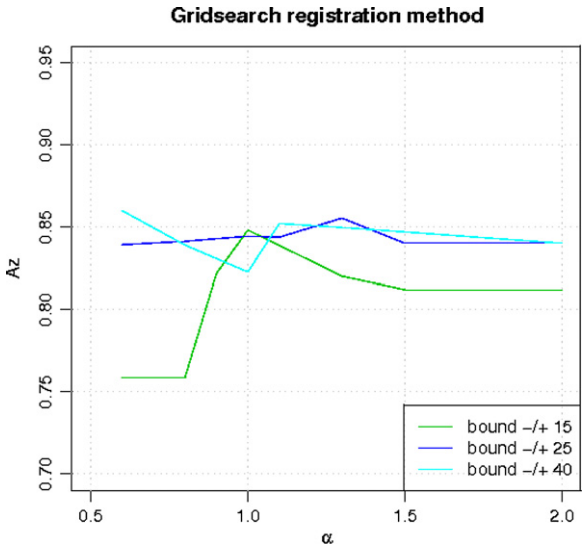

Figure 6. Parameters grid search for the B-spline registration, with bound (B), the optimizer constraint on the displacement of the control points, α the Jacobian factor and Az the diagnostic performance of the CADx system.

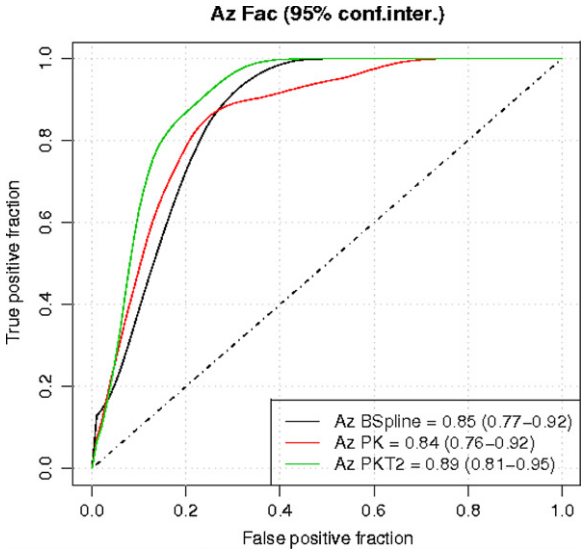

Figure 7. ROC curves showing the diagnostic performance of the CADx system using the T2 estimates after non-rigid registration, versus only using PK parameters and the additional value of T2 estimates when they are combined with the PK parameters.

($r = 0.97$, $p = 0.001$). Finally, adding the T2 values as feature to the CADx system resulted in a significantly improved discriminating performance of 0.89 (0.81–0.95), compared to only using the PK features (0.84 (0.76–0.92)). The performance increase agrees well with the

previous literature on combining T2 estimates and PK parameters (Hricak *et al* 2007, Futterer *et al* 2006, Chan *et al* 2003).

The calculated T2 relaxation times for the prostate (82 ± 7.5 ms) were compared with those found in the literature. In the small study of de Bazelaire *et al* (2004) (based on data from three healthy men), prostate and vertebra relaxation rates of 88 ± 0 ms were calculated. Chan *et al* (2003) found relaxation rates of 128.3 ± 42.9 ms for nonbrachytherapy patients and 88 ± 21 ms for post-brachytherapy patients in the normal PZ. More recently Roebuck *et al* (2009), using a different T2 map imaging sequence, found, in 18 men with biopsy-proven PCa, relaxation rates of 193 ± 49 ms in healthy tissue and 100±26 ms in suspected cancer. Liney *et al* (1997) found in an early study relaxation rates of 96.2 ± 15.2 ms in patients but in a more recent study 135.5 ± 40.0 ms in the normal PZ of patients (Gibbs *et al* 2001). Two observations can be made from this literature survey. First, there is no consensus on the absolute T2 value of normal PZ. Consequently, any T2 discrimination protocol or CADx system has to account for the T2 estimation method that was used. Secondly, a large inter-patient variability. The presented method has a much lower variability, which partly explains the good discriminative properties of the estimated T2 relaxation times. The reduced variability may be explained by the use of reference tissue (section 2.5). In doing so, the method calibrates on a per patient basis which may be better in capturing machine dependences. The effect of using calibration on the diagnostic performance was also demonstrated in a previous study (Vos *et al* 2007), but then in a pharmacokinetic context.

The T2 estimator has a number of potential shortcomings. First, muscle T2 variability can result in different T2 estimates, as it is used as reference tissue. The variability is an effect of physical activity and muscle training. In this study, we used the levator ani muscle as reference tissue. In contrast to most skeletal muscles, levator ani muscles are non-voluntary; therefore, intra-patient T2 variation is small. Secondly, the method is sensitive to B1 fluctuations. The volume of interest (prostate region), however, is in the middle of the image where B1 fluctuations are less present. Thirdly, the T2-w tse sequence has contributed data from different echo times (depending on the echo train length and *k*-space sampling) and therefore the estimated T2 values might not be in exact concordance with a multi-echo spin echo-derived estimation. The slight inaccuracy, however, will be evident in all patients and all tissues evaluated. The inaccuracy will be compensated for by using reference tissue calibration (e.g., muscle). Fourthly, the T2-w and PD-w coil setup should be identical.

The current study has a number of limitations. One limitation is the amount of time needed for the non-rigid registration, which now ranges from 5 min to 15 min. This, however, will not conflict the intended application since the radiologist does not evaluate the images directly after the acquisition and the registration can thus be performed offline. A second limitation is the manual annotation of the levator ani muscle, which is needed for the reference tissue method. One solution is to have more information on actual gain coefficients and sequence models used by the MR system. Yet the reference tissue method may have a positive effect on the discriminating performance as stated above. Another potential method would be an automated segmentation of the levator ani muscle and is part of further research. Nevertheless, manual segmentation of the muscle and computation of the T2 estimates are performed in seconds. Third limitation is that the registration method parameter Jacobian constraint weight (α) requires tuning (figure 6). Different MR hardware (e.g., at 3 Tesla) and sequence settings may require different parameter settings.

In conclusion, the study demonstrated a simple T2 estimation method that has a diagnostic performance such that it complements a DCE T1-w-based CADx system in discriminating malignant lesions from normal and benign regions with a significant improved accuracy of 0.89 (0.81–0.95) compared to those only using DCE-derived features.

Acknowledgments

This work was funded by grant KUN 2004-3141 of the Dutch Cancer Society.

References

Chan I, Wells W 3rd, Mulkern R V, Haker S, Zhang J, Zou K H, Maier S E and Tempany C M 2003 Detection of prostate cancer by integration of line-scan diffusion, T2-mapping and T2-weighted magnetic resonance imaging: a multichannel statistical classifier *Med. Phys.* **30** 2390–8

Collins D J and Padhani A R 2004 Dynamic magnetic resonance imaging of tumor perfusion. Approaches and biomedical challenges *IEEE Eng. Med. Biol. Mag.* **23** 65–83

de Bazelaire C M, Duhamel G D, Rofsky N M and Alsop D C 2004 MR imaging relaxation times of abdominal and pelvic tissues measured *in vivo* at 3.0 T: preliminary results *Radiology* **230** 652–9

Engelbrecht M R, Huisman H J, Laheij R J, Jager G J, van Leenders G J, Hulsbergen-Van De Kaa C A, de la Rosette J J, Blickman J G and Barentsz J O 2003 Discrimination of prostate cancer from normal peripheral zone and central gland tissue by using dynamic contrast-enhanced MR imaging *Radiology* **229** 248–54

Futterer J J *et al* 2006 Prostate cancer localization with dynamic contrast-enhanced MR imaging and proton MR spectroscopic imaging *Radiology* **241** 449–58

Gibbs P, Tozer D J, Liney G P and Turnbull L W 2001 Comparison of quantitative T2 mapping and diffusion-weighted imaging in the normal and pathologic prostate *Magn. Reson. Med.* **46** 1054–8

Gold G E, Han E, Stainsby J, Wright G, Brittain J and Beaulieu C 2004 Musculoskeletal MRI at 3.0 T: relaxation times and image contrast *AJR Am. J. Roentgenol.* **183** 343–51

Hittmair K, Gomiscek G, Langenberger K, Recht M, Imhof H and Kramer J 1994 Method for the quantitative assessment of contrast agent uptake in dynamic contrast-enhanced MRI *Magn. Reson. Med.* **31** 567–71

Hornik K 2005 *The R FAQ* http://CRAN.R-project.org/doc/FAQ

Hricak H, Choyke P L, Eberhardt S C, Leibel S A and Scardino P T 2007 Imaging prostate cancer: a multidisciplinary perspective *Radiology* **243** 28–53

Huisman H J, Engelbrecht M R and Barentsz J O 2001 Accurate estimation of pharmacokinetic contrast-enhanced dynamic MRI parameters of the prostate *J. Magn. Reson. Imaging* **13** 607–14

Klein S, Staring M and Pluim J P 2007 Evaluation of optimization methods for nonrigid medical image registration using mutual information and B-splines *IEEE Trans. Image Process.* **16** 2879–90

Liney G P, Turnbull L W, Lowry M, Turnbull L S, Knowles A J and Horsman A 1997 *In vivo* quantification of citrate concentration and water T2 relaxation time of the pathologic prostate gland using 1H MRS and MRI *Magn. Reson. Imaging* **15** 1177–86

Mulkern R V, Rybicki F J, Haker S J and Tempany C M 2004 Comments on T2 measurements of prostate tissue *Radiology* **232** 624–5 (author reply 625–6)

Madabhushi A, Feldman M D, Metaxas D N, Tomaszeweski J and Chute D 2005 Automated detection of prostatic adenocarcinoma from high-resolution *ex vivo* MRI *IEEE Trans. Med. Imaging* **24** 1611–25

Maes F, Collignon A, Vandermeulen D, Marchal G and Suetens P 1997 Multimodality image registration by maximization of mutual information *IEEE Trans. Med. Imaging* **16** 187–98

Mattes D, Haynor D R, Vesselle H, Lewellen T K and Eubank W 2003 PET-CT image registration in the chest using free-form deformations *IEEE Trans. Med. Imaging* **22** 120–8

Padhani A R 2003 MRI for assessing antivascular cancer treatments *Br. J. Radiol.* **76** S60–80

Pluim J P, Maintz J B and Viergever M A 2003 Mutual-information-based registration of medical images: a survey *IEEE Trans. Med. Imaging* **22** 986–1004

Rohlfing T, Maurer C R Jr, Bluemke D A and Jacobs M A 2003 Volume-preserving nonrigid registration of MR breast images using free-form deformation with an incompressibility constraint *IEEE Trans. Med. Imaging* **22** 730–41

Roebuck J R, Haker S J, Mitsouras D, Rybicki F J, Tempany C M and Mulkern R V 2009 Carr–Purcell–Meiboom–Gill imaging of prostate cancer: quantitative T(2) values for cancer discrimination *Magn. Reson. Imaging* **27** 497–502

Rueckert D, Sonoda L I, Hayes C, Hill D L, Leach M O and Hawkes D J 1999 Nonrigid registration using free-form deformations: application to breast MR images *IEEE Trans. Med. Imaging* **18** 712–21

Rutter C M 2000 Bootstrap estimation of diagnostic accuracy with patient-clustered data *Acad. Radiol.* **7** 413–9

Studholme C, Hill D L and Hawkes D J 1997 Automated three-dimensional registration of magnetic resonance and positron emission tomography brain images by multiresolution optimization of voxel similarity measures *Med. Phys.* **24** 25–35

Thévenaz P and Unser M 2000 Optimization of mutual information for multiresolution image registration *IEEE Trans. Image Process.* **9** 2083–99

Viswanath S, Bloch B N, Genega E, Rofsky N, Lenkinski R, Chappelow J, Toth R and Madabhushi A 2008 A comprehensive segmentation, registration, and cancer detection scheme on 3 Tesla *in vivo* prostate DCE-MRI *Med. Image Comput. Comput. Assist. Interv.* **11** (Pt 1) 662–9

Vos P C, Hambrock T, Futterer J J, Hulsbergen-Van De Kaa C A, Barentsz J O and Huisman H J 2007 Effect of calibration on computerized analysis of prostate lesions using quantitative dynamic contrast-enhanced magnetic resonance imaging *Medical Imaging 2007: Computer-Aided Diagnosis; Proc. SPIE* **6514** 65140U

Vos P C, Hambrock T, Hulsbergen-van de Kaa C A, Futterer J J, Barentsz J O and Huisman H J 2008a Computerized analysis of prostate lesions in the peripheral zone using dynamic contrast enhanced MRI *Med. Phys.* **35** 888–99

Vos P C, Hambrock T, Barentsz J O and Huisman H J 2008b Combining T2-weighted with dynamic MR images for computerized classification of prostate lesions *Medical Imaging 2008: Computer-Aided Diagnosis; Proc. SPIE* **6915** 69150W

Wells W M 3rd, Viola P, Atsumi H, Nakajima S and Kikinis R 1996 Multi-modal volume registration by maximization of mutual information *Med. Image Anal.* **1** 35–51

Zhu C, Byrd R H and Nocedal J 1997 L-bfgs-b: algorithm 778: L-bfgs-b, fortran routines for large scale bound constrained optimization *ACM Trans. Math. Softw.* **23** 550–60